Cholesterol stimulates the lytic activity of Adenylate Cyclase Toxin on lipid membranes by promoting toxin oligomerization and formation of pores with a greater effective size

David González Bullón, Kepa B. Uribe, Jone Amuategi, César Martín and Helena Ostolaza [ID]

Department of Biochemistry and Molecular Biology, Biofisika Institute, (UPV/EHU, CSIC), University of Basque Country (UPV/EHU), Bilbao, Spain

Several toxins acting on animal cells present different, but specific, interactions with cholesterol. *Bordetella pertussis* infects the human respiratory tract and causes whooping cough, a highly contagious and resurgent disease. Its virulence factor adenylate cyclase toxin (ACT) plays an important role in the course of infection. ACT is a pore-forming cytolysin belonging to the Repeats in ToXin (RTX) family of leukotoxins/hemolysins and is capable of permeabilizing several cell types and lipid vesicles. Previously, we observed that in the presence of cholesterol ACT induces greater liposome permeabilization. Similarly, recent reports also implicate cholesterol in the cytotoxicity of an increasing number of pore-forming RTX toxins. However, the mechanistic details by which this sterol promotes the lytic activity of ACT or of these other RTX toxins remain largely unexplored and poorly understood. Here, we have applied a combination of biophysical techniques to dissect the role of cholesterol in pore formation by ACT. Our results indicate that cholesterol enhances the lytic potency of ACT by promoting toxin oligomerization, a step which is indispensable for ACT to accomplish membrane permeabilization and cell lysis. Since our experimental design eliminates the possibility that this cholesterol effect derives from toxin accumulation due to lateral lipid phase segregation, we hypothesize that cholesterol facilitates lytic pore formation, by favoring a toxin conformation more prone to protein–protein interactions and oligomerization. Our data shed light on the complex relationship between lipid membranes and protein toxins acting on these membranes. Coupling cholesterol binding, increased oligomerization and increased lytic activity is likely pertinent for other RTX cytolysins.

Introduction

Cholesterol is an essential component of the plasma membrane of most eukaryotic cells, where it is nonrandomly distributed, and plays a crucial role in membrane organization, dynamics, and function [1-3]. Beyond its well-documented effects on the physical state of the phospholipid bilayer, cholesterol has been

reported to be necessary for the function of many membrane proteins [4,5]. The crucial role of cholesterol in facilitating structural rearrangements of proteins upon association with the lipid bilayer, resulting in the spontaneous conversion of the protein from water-soluble to membrane-bound form has been documented. This cholesterol-dependent membrane insertion is a widely observed phenomenon and occurs in several bacterial pore-forming toxins (PFTs), as well as in other human proteins such as perforin, or members of the complement membrane attack complex [4]. In a previous study, we revealed that cholesterol regulates the pore-forming activity of the adenylate cyclase toxin (ACT or CyaA) on model membranes [5].

Adenylate cyclase toxin is a key virulence factor of *Bordetella pertussis* and plays a critical role during the initial steps of the respiratory tract colonization by the pathogen [6,7]. The toxin targets primarily myeloid phagocytic cells that express the CD11b/CD18 toxin receptor, and induces phagocyte impotence [8,9]. ACT belongs to the so-called Repeats in ToXin (RTX) family of bacterial proteins, characterized by possessing several calcium-binding, glycine-, and aspartate-rich nonapeptide repeats at the C-terminal end of their sequences [10,11]. Among the RTX proteins with cytotoxic and cytolytic function, ACT is unique in that its 1706 residues-long polypeptide chain consists of an N-terminal ~ 400 residue-long adenylate cyclase enzyme domain (AC domain) fused to a characteristic RTX hemolysin moiety of ~ 1200 residues through a ≈ 100 residue-long linker segment (translocation region) [12,13]. The hemolysin moiety itself consists of several functional regions: a pore-forming region (residues ≈ 500–700) with several amphiphatic/hydrophobic alpha-helices involved in membrane insertion; an activation region, with two posttranslationally acylated lysine residues (Lys 860 and Lys 983) [14,15]; a calcium-binding domain containing about ~ 40 typical RTX nonapeptide repeats [16,17]; and a nonprocessed C-terminal secretion signal recognized by T1SS [18].

Cytotoxicity by ACT results from the synergy between the two main activities of the toxin, production into the target cytosol of supraphysiological cAMP levels upon delivery of its adenylate cyclase domain (AC domain), and cell membrane permeabilization, induced by its pore-forming domain (hemolysin domain), which debilitate the host defenses [19].

It has been proposed that translocation of the AC domain into cells and formation of toxin pores are two independent, and mutually exclusive, activities of ACT, that would be accomplished by two different toxin conformers, one leading to translocation and other leading to hemolysis [20]. Translocation of the catalytic domain into target cytosol appears to be a linear function of toxin concentration, which suggests that monomeric ACT is involved in AC domain delivery [21], and it has been proposed that it takes place in cholesterol- and SM-enriched lipid nanodomains [22]. However, hemolysis of erythrocytes by ACT was reported to be a higher-order function of toxin concentration, with a Hill cooperativity number ≥ 3 [21], suggesting that assembly of several toxin molecules is involved in pore formation by ACT. It was reported that such oligomeric ACT pores were cation-selective proteinaceous pores of very small size with ≈ 0.6–0.8 nm of diameter [23]. More recently, our laboratory has provided the first nanoscale visualization of oligomeric ACT lytic 'holes' into lipid membranes [24], showing that ACT forms heterogeneous oligomeric assemblies of several nanometers wide and proteolipidic characteristics, and not of fixed size small pores as previously believed.

Resembling other pore-forming proteins, it can be anticipated that pore formation by ACT involves also several consecutive steps (binding, insertion and assembly) leading to these lytic oligomers. So far, more effort has been dedicated to discern and define protein segments distinctively involved in each toxin activity and that would hence lead to distinguish each putative toxin conformer. However, the possible determinants of the cell membrane itself, and how these, might regulate the several steps leading to pore formation and toxin lytic capacity remain poorly known. From leakage experiments involving liposomes of different lipid composition, we showed previously that cholesterol increases the permeabilization ability of ACT [5].

In the present study, we have employed several biophysical techniques such as atomic force microscopy, confocal microscopy, and lipid monolayers to explore in detail the effect of cholesterol on the lytic capacity of ACT. For comparative purposes, we have used two lipid compositions, namely, dioleylphosphatidylcholine (DOPC) and mixtures of DOPC with different proportions of cholesterol (3 : 1, 2 : 1, and 1 : 1 molar ratios). Pure DOPC vesicles represent the fluid, liquid disordered (Ld or Lα), bulk lipid phase of the cell membrane, while DOPC:Chol (1 : 1 molar ratio) lipid mixture adopts a single liquid ordered (Lo or Lβ) phase, with tightly packed lipids and greater thickness [43], mimicking, somehow, the more rigid Lo nanodomains enriched in SM and cholesterol ('rafts') that are believed to form in natural membranes [44-46]. Our results indicate that interaction of ACT with cholesterol favors toxin insertion and oligomerization, likely by favoring a toxin conformation more prone to stablish protein-protein interactions necessary for toxin

assembly, this way stimulating the lytic activity of ACT. Enhancement in the conversion of soluble pore-forming toxins to their membrane-inserted state may thus be a common effect of membrane cholesterol.

Results

Cholesterol enhances the extent and rate of LUV permeabilization by ACT

To study the effect of cholesterol on the lytic activity of ACT in membranes, we performed firstly permeabilization experiments with the broadly used method of content release using the ANTS/DPX dye pair encapsulated into large unilamellar liposomes (LUVs). ANTS (8-aminonaphthalene-1,3,6-trisulfonic acid) is the fluorophore and DPX (*p*-xylene-bis-pyridinium bromide) is a cationic quencher. As the liposome is permeabilized by the pore-forming toxin, the ANTS and DPX probes are released from the vesicle interior and diffuse apart, and the resultant increase in fluoresce signal is detected in a spectrofluorimeter. Fig. 2 shows the results of representative time course experiments performed with LUVs of DOPC containing increasing sterol concentrations (DOPC:Chol 1 : 0, 3 : 1, 2 : 1, and 1 : 1 molar ratios) and treated with different ACT doses (10–400 nM). Fluorescence data in the individual time course experiments were collected for 30 min.

The percentages of vesicle permeabilization calculated for each lipid composition and each toxin dose, expressed as mean values $\pm$ SD of at least three independent assays, have been depicted in Fig. 1A. From data in Figs 1A and 2, it was evident that incorporation of cholesterol in the DOPC vesicles had a notable enhancing effect on two characteristic permeabilization parameters, the extent, and the rate of permeabilization. The enhancing effect was directly proportional to the sterol amount in the LUVs and evident for all the toxin concentrations tested. This effect of cholesterol was more easily evidenced by comparing the D_{50} (the ACT concentration required to induce 50% permeabilization of the LUVs) and t_{50} (time required to induce the 50% permeabilization for a toxin concentration of 100 nM) values for the different lipid compositions (Figs 1B, C). As compared to the pure DOPC liposomes, the presence of cholesterol notably decreased the D_{50} value, with maximal effect achieved for 50% cholesterol, which decreased about ten times the amount of toxin required to induce 50% permeabilization (Fig. 1B). Interestingly, in previous studies of hemolysis by ACT, the reported toxin concentrations required to induce 50% lysis of erythrocytes were

rather similar to the D_{50} obtained here for the DOPC: Chol 1 : 1 liposomes ($D_{50} = 15$ nM) [19]. This suggests, somehow, that the phospholipid vesicles containing moderate-high amounts of cholesterol may become almost as sensitive as red blood cells to ACT lytic activity. Incorporation of cholesterol in the vesicles had also a prominent effect on the leakage kinetics, reducing progressively the t_{50} values as the amount of sterol increases (Fig. 1C). For example, the t_{50} value calculated for DOPC:Chol 1 : 1 liposomes treated with 100 nM ACT ($t_{50} \approx 200$ s) was about one order of magnitude faster than the t_{50} determined for pure DOPC liposomes ($t_{50} > 1800$ s) (Fig. 1C). These data thus suggest that the greater is the cholesterol content of the vesicle, the smaller is the amount of toxin required, and the faster are permeabilized the LUVs by ACT.

Cholesterol increases ACT binding to lipid vesicles and subsequent toxin oligomerization

Cholesterol may affect different steps (binding, insertion, oligomerization, etc.) involved in protein-membrane or protein–protein interaction leading to permeabilization. Representing graphically the increment in the percentage leakage (Δleakage) resulting from the incorporation of different amounts of cholesterol (25, 33, and 50%) in the LUVs, relative to the percentage leakage obtained for the pure DOPC liposomes (data taken from Fig. 1 A), at each toxin concentration tested, one can have an idea of whether the enhancing effect of cholesterol on leakage is homogeneous in the whole range of ACT concentrations tested, or not, and from this, it can be inferred whether cholesterol is affecting toxin binding to the vesicles. Fig. 3 shows that at high toxin doses (toxin input > 100 nM), ACT is able to disrupt both types of vesicles (with and without cholesterol) with almost the same efficiency, perhaps because the bilayer is saturated with toxin. However, as the toxin concentration became lower, the presence of cholesterol in the vesicles markedly improved the permeabilization capacity of ACT relative to the pure DOPC liposomes, almost tripling the permeabilization extent in the presence of 50% cholesterol, as compared with pure DOPC. This result suggests that cholesterol plays a critical role that is evidenced especially at low toxin concentrations. Since lysis by ACT pore-forming activity involves assembly of toxin monomers into the membrane [21,24,25], these data strongly suggest that ACT might require a critical monomer concentration at the membrane to oligomerize. Cholesterol, by increasing ACT binding to the membrane, might facilitate achievement of such minimal number of toxin molecules at lower initial ACT inputs,
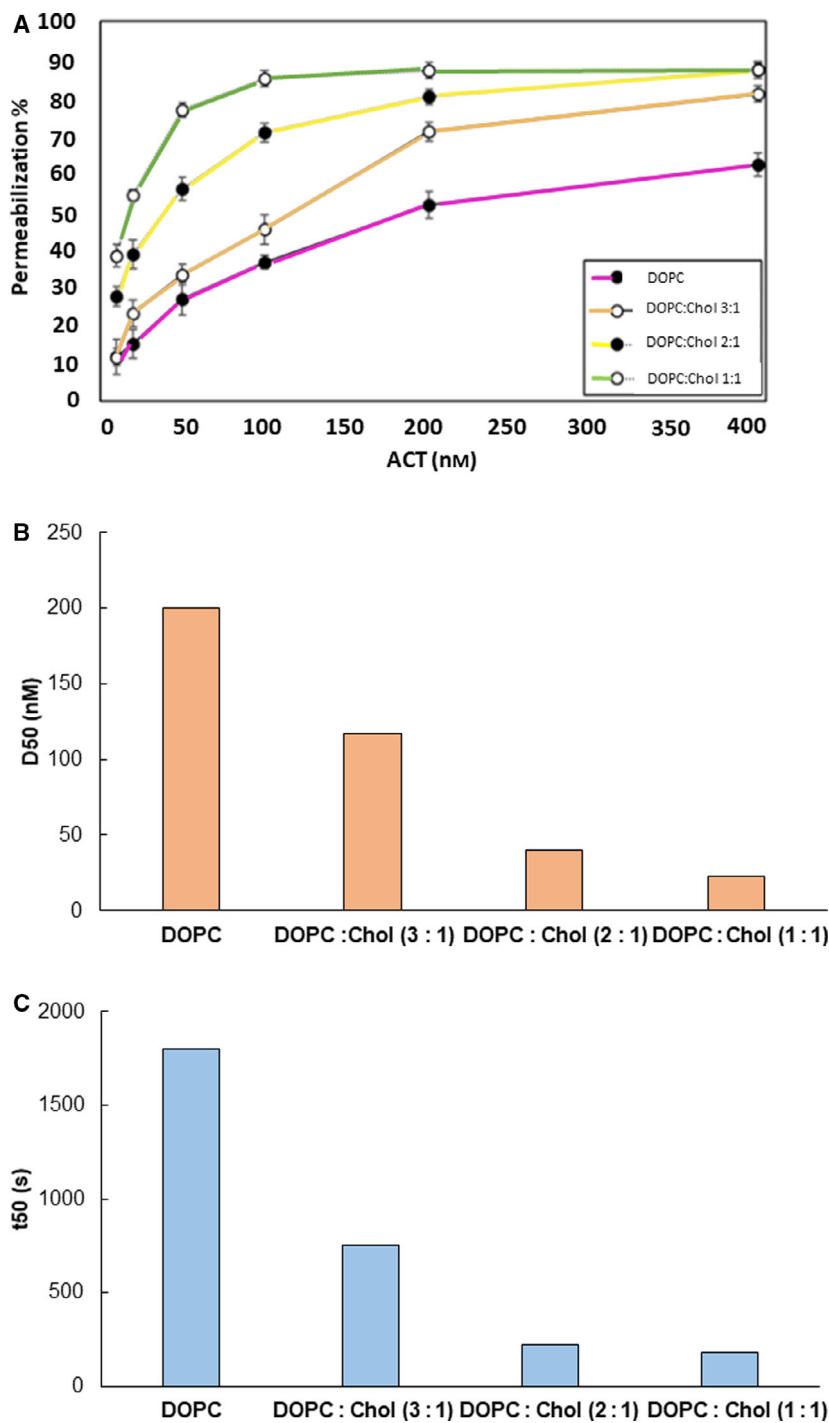
Fig. 1. Cholesterol importantly enhances both the extent and the rate of LUV permeabilization by ACT, proportionally to the amount of sterol present in the lipid membranes. (A) The percentages of vesicle permeabilization for each lipid composition (DOPC, DOPC:Chol 3 : 1, DOPC:Chol 2 : 1, or DOPC:Chol 1 : 1, expressed as molar ratios) and each toxin dose in the range 10–400 nM were calculated from individual time course experiments as the depicted in Fig. S1, and expressed as mean values $\pm$ SD of at least three independent assays. Fluorescence data in the time course experiments were collected for 30 min. (B) D_{50} (nM) values, representing the ACT concentration required to induce 50% LUVs permeabilization, are represented for each lipid composition. (C) t_{50} values corresponding to the time required to induce the 50% of permeabilization of the liposomes are represented for each lipid composition. The D_{50} and t_{50} values were calculated from leakage experiments similar to the shown in Fig. 2.

favoring this way toxin oligomerization and consequently vesicle permeabilization.

This enhancing effect of cholesterol on toxin binding to liposomes was confirmed qualitatively by performing BN-PAGE and immunoblotting of DOPC or DOPC:Chol (1 : 1 molar ratio) liposomes (100 μM) incubated for 30 min at 37° with ACT (50 nM)

(Fig. 4). Upon incubation, the unbound toxin was eliminated and the toxin-treated liposomes collected by means of a vesicle flotation assay following centrifugation in a sucrose gradient (see Material and Methods). The figure shows indeed that for the same initial toxin input the relative intensity of the protein bands resolved in the BN-PAGE gel is substantially greater
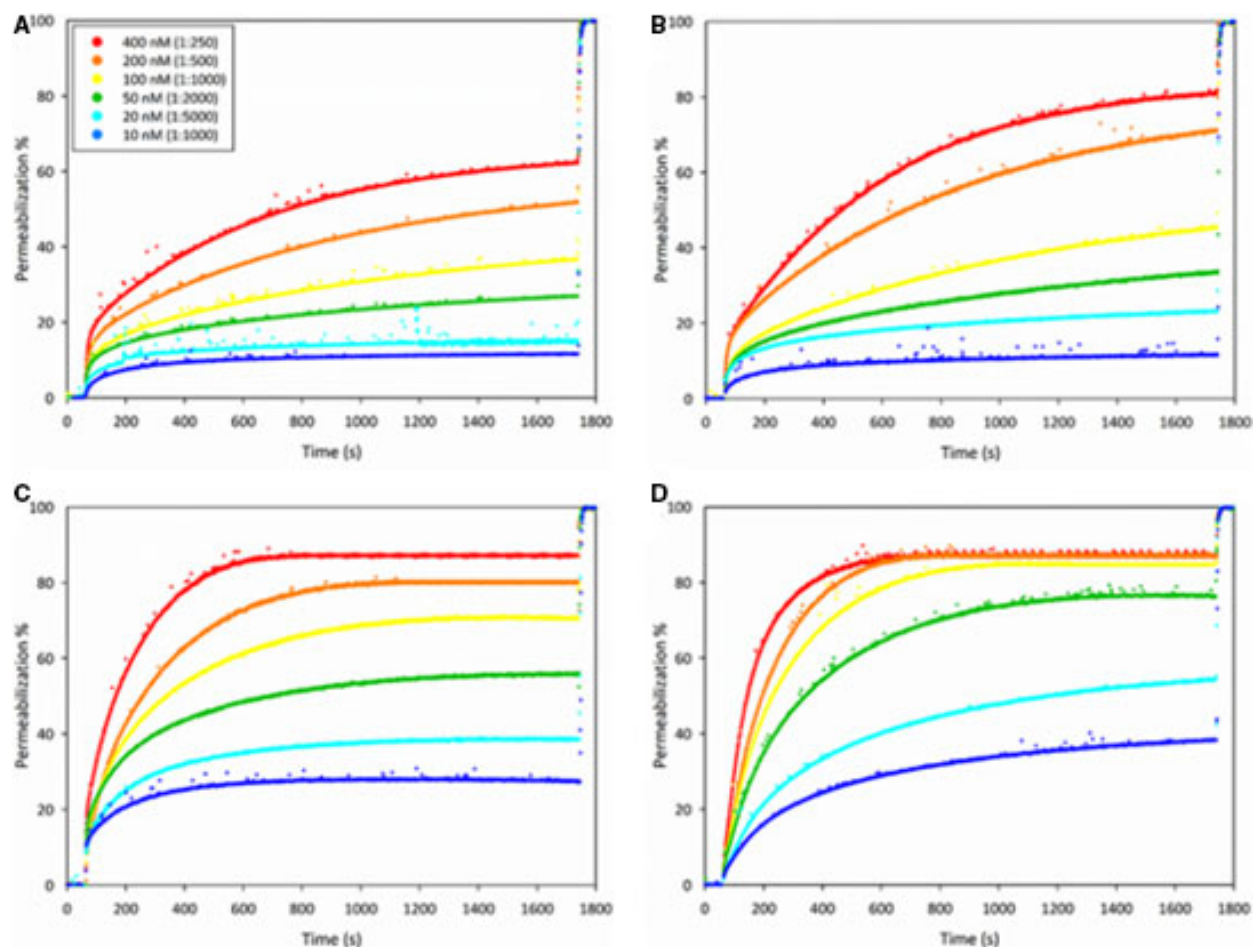
Fig. 2. Time course recordings of the release of vesicle aqueous contents by ACT pore-forming activity. The figure shows representative raw kinetics of LUV permeabilization by ACT measured as release of encapsulated ANTX/DPX fluorescent probes from large unilamellar DOPC liposomes with different cholesterol content. Liposomes, at a final lipid concentration of 100 μM, and the following lipid compositions, DOPC (A), DOPC:Chol 3 : 1 (molar ratio) (B), DOPC:Chol 2 : 1 (molar ratio) (C), and DOPC:Chol 1 : 1 (molar ratio) (D), were incubated with ACT at different toxin concentrations within the 10–400 nM range, in 150 mM NaCl, 20 mM Tris, 10 mM CaCl$_2$, pH8 assay buffer, at 37 °C, under constant stirring. Release of ANTS was followed in a *Fluorolog-3* spectrofluorimeter using λex = 360 nm and λem = 520 nm. ACT, at the desired concentration, was added 60 s after initiating the fluorescence emission recording. 100% release was achieved by adding Triton X-100 at 0.1% to the simple.

in the vesicles containing 50% cholesterol as compared with the pure DOPC LUVs, suggesting thus a greater ACT binding to the sterol-containing vesicles. In addition, in the cholesterol-containing liposomes three major multimeric protein bands with apparent molecular masses compatible with ACT trimers, tetramers, and hexamers (apparent size of the ACT monomer ≈ 200 kDa) are clearly visible, whereas in the DOPC liposomes the multimeric protein bands are only two (compatible with ACT trimers and hexamers) and are less intense.

We designed an additional assay to verify that cholesterol increases ACT binding to liposomes. In this experiment, the toxin (50 nM) was first pre-incubated

for 30 min at 37 °C with DOPC or DOPC:Chol (1 : 1 molar ratio) LUVs at three different lipid concentrations (0.1 mM, 0.2 mM, and 1 mM). After this incubation, erythrocytes were added, and hemolysis by ACT was examined. Data in Fig. 5 show that the final extent of ACT-induced hemolysis results diminished when ACT is pre-incubated with both types of liposomes, and that this effect was proportional to the final lipid concentration used in the pre-incubation. The drop of the hemolysis extent was more pronounced for the cholesterol-containing liposomes as compared to the pure DOPC LUVs. For example, pre-incubation of ACT (50 nM) with 1 mM DOPC LUVs allowed about 50% of the maximal hemolysis
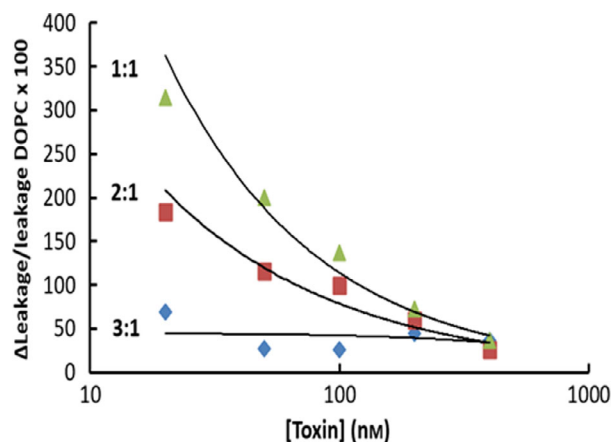
Fig. 3. The effect of cholesterol enhancing permeabilization by ACT is more pronounced at the lower toxin concentrations, suggesting that cholesterol favors ACT oligomerization. In the figure, it has been represented graphically the increment in the percentage leakage (Δleakage) resulting from the incorporation of different amounts of cholesterol (25, 33, and 50%) in the LUVs, relative to the percentage leakage obtained for the pure DOPC liposomes (data taken from Fig. 1), at each toxin concentration tested. Leakage data for each toxin concentration and lipid composition were taken from Fig. 1.

Fig. 4. Analysis by BN-PAGE and immunoblotting of DOPC or DOPC:Chol (1 : 1 molar ratio) liposomes treated with ACT reveals greater toxin multimerization in the presence of the sterol. The presence of possible multimeric ACT assemblies was detected by blue-native electrophoresis (BN-PAGE) of ACT-treated DOPC or DOPC:Chol (1 : 1 molar ratio) large unilamellar liposomes. The lipid vesicles (final lipid concentration 100 μM) were incubated with the toxin (50 nM) for 30 min at 37 °C, then samples were processed to remove the unbound toxin, and then run in a blue native gel (3– 12% acrylamide gradient) and the corresponding blotted membrane was stained with an anti-ACT MAb (9D4) monoclonal antibody.

(obtained with 50 nM ACT without pre-incubation with LUVs), whereas the incubation with the same concentration of DOPC:Chol (1 : 1 molar ratio) LUVs, almost abrogated the ACT-induced hemolysis, most likely because more ACT binds irreversibly to the DOPC:Chol vesicles, and thus, less free toxin is available to bind and lyse the red blood cells. A direct binding assay of ACT to DOPC and DOPC:Chol (1 : 1 molar ratio) liposomes fully corroborated that substantially more toxin binds to the cholesterol-containing vesicles (Fig. 6).

ACT forms dynamic pores with greater effective size in cholesterol-containing giant unilamellar liposomes

To investigate in more detail whether cholesterol affects the characteristics of the ACT pores or the mechanism of pore formation, we applied the single giant unilamellar vesicle (GUV) methodology [26,27]. Previously, we had used this same methodology to characterize ACT-induced permeabilization and the mechanisms of pore formation by the toxin, and we proved that it reflects the calcium-dependent pore-forming activity of ACT on membranes [24]. The single-vesicle method is based on the analysis by confocal microscopy of the influx of fluorescently labeled solutes (that can be of different sizes)
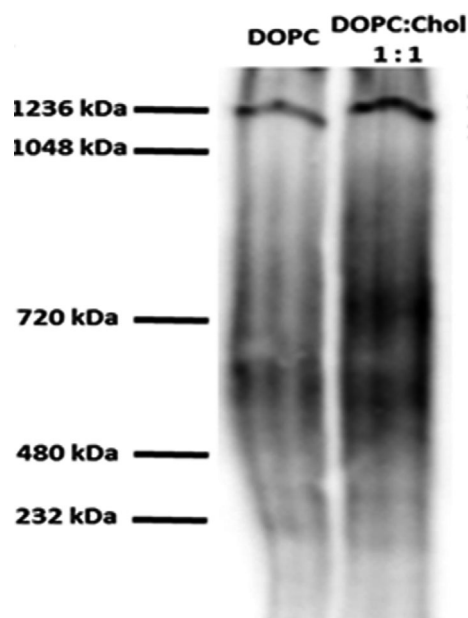
from the external medium into the lumen of the GUVs. Since the assay with GUVs allows the direct detection of individual vesicles, it provides more accurate estimations of the effective size (internal diameter) of the pores.

Fig. 7 shows individual images from representative independent experiments, in which DOPC:Chol 1 : 1 GUVs were treated for 30' (subpanels a to g) or 60' (subpanels g to m) at RT with a single ACT dose (200 nM). This toxin concentration is in the interval commonly used in hemolysis assays by ACT [19], and similar to the doses used in the laboratory in leakage experiments from LUVs or GUVs [24]. In each experiment, the external solution bathing the GUVs contained one of the following fluorophore: Alexa-Fluor-488, or one of the five FITC-labeled dextrans of different molecular mass (4 kDa-FITC-Dextran, 10 kDa-FITC-Dextran, 20 kDa-FITC-Dextran, 40 kDa-FITC-Dextran, or 70 kDa-FITC-Dextran) all of them detected as green-colored fluorescence. Rhodamine-PE (0.5%) (red color) was included in all cases to label the lipid
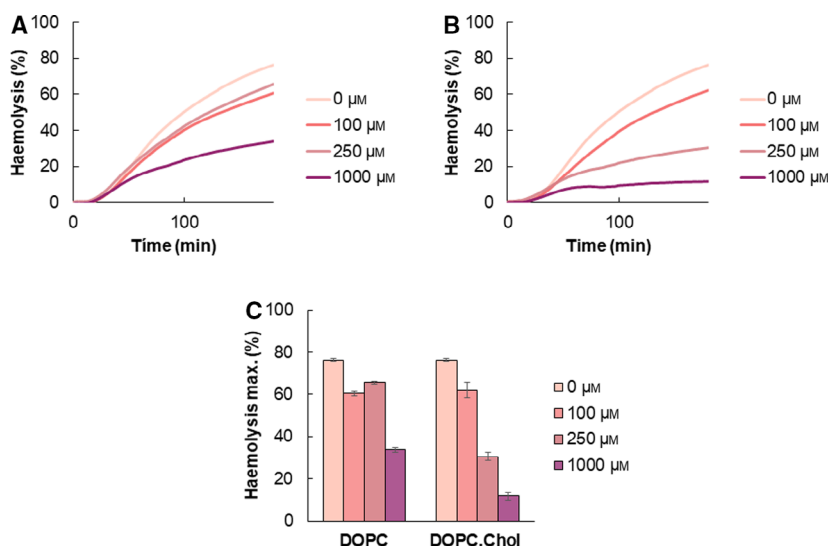
Fig. 5. ACT-induced hemolysis of sheep erythrocytes after initial pre-incubation of the toxin with liposomes of different lipid composition. ACT (50 nM) was firstly pre-incubated for 30 min at 37°C with DOPC or DOPC:Chol (1 : 1 molar ratio) LUVs at three different lipid concentrations (0.1 mM, 0.25 mM, and 1 mM). Immediately after this incubation, sheep erythrocytes (5 × 10^8 cells·mL^{-1}) were added, and hemolysis by ACT was examined. Subpanels (a) and (b) show raw representative recordings of hemolysis by ACT pre-incubated with DOPC LUVs at different concentrations and the control without toxin, or pre-incubated with DOPC:Chol (1 : 1 molar ratio) at the same concentrations, respectively, depicted as release of hemoglobin and expressed as percentages. Subpanel (c) shows the percentages of hemolysis calculated after 180 min of toxin incubation with the red blood cells. Data depicted in this subpanel correspond to mean values ± SD. Three independent experiments were performed in duplicates (*n* = 6).
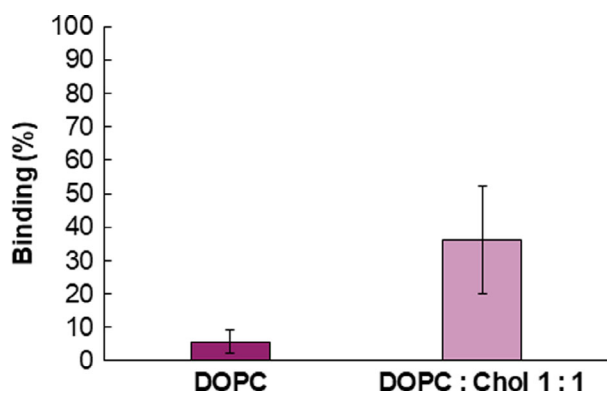

Fig. 6. Binding of ACT to large unilamellar vesicles with different lipid composition. DOPC or DOPC:Chol (1 : 1 molar ratio) liposomes labeled with PE-Rhodamine (0.5%) were incubated for 30 min with ACT toxin at a lipid:protein molar ratio of 2000 : 1. Upon incubation, the unbound toxin was separated from the vesicles with bound toxin by a flotation assay in sucrose gradient centrifugation. Liposome-associated AC activity was then determined (binding) for each type of liposomes. Activities are expressed as percentages of intact free toxin activity and represent average values ± S.D. from three independent experiments.

bilayer of the GUVs. As shown in Fig. 7, control GUVs are seen in black color (subpanels a, and h), since in the absence of toxin the membrane remains impermeable to the external fluorophore (green color), and consequently, the vesicles do not contain fluorescent probe inside. Instead, upon ACT treatment the membrane is permeabilized by toxin pores. This leads to the influx of the corresponding external fluorescent molecule into the GUVs lumen, which becomes green-colored.

As shown in Fig. 7 after the first 30-min incubation, the cholesterol-containing GUVs were permeable either to the smaller fluorescent solutes (Alexa-Fluor 488 and 4 kDa FITC-Dextran) (subpanels b, c) as to the 10 kDa and 20 kDa FITC-Dextrans (subpanels d, e). Prolonging the incubation time from 30 min to 1h the size of the fluorescent solutes that could enter into the vesicles increased (subpanels g to m). After 60', even solutes of very large sizes such as 40 kDa and 70 kDa FITC-Dextrans entered into the ACT-treated vesicles (subpanels l, m). The estimated molecular radii for the larger dextrans are 4.5 nm for the 40 kDa FITC-Dextran, and 6.0 nm for the 70 kDa FITC-Dextran, meaning that the 'effective' size of the 'lesions' formed by ACT in the DOPC:CHOL (1 : 1 mol ratio) GUVs upon 1h at RT could exceed even the 12 nm of diameter. This pore size is comparable to the large oligomeric pores formed by several cholesterol-dependent cytolysins such as listeriolysin or streptolysin [4,28].
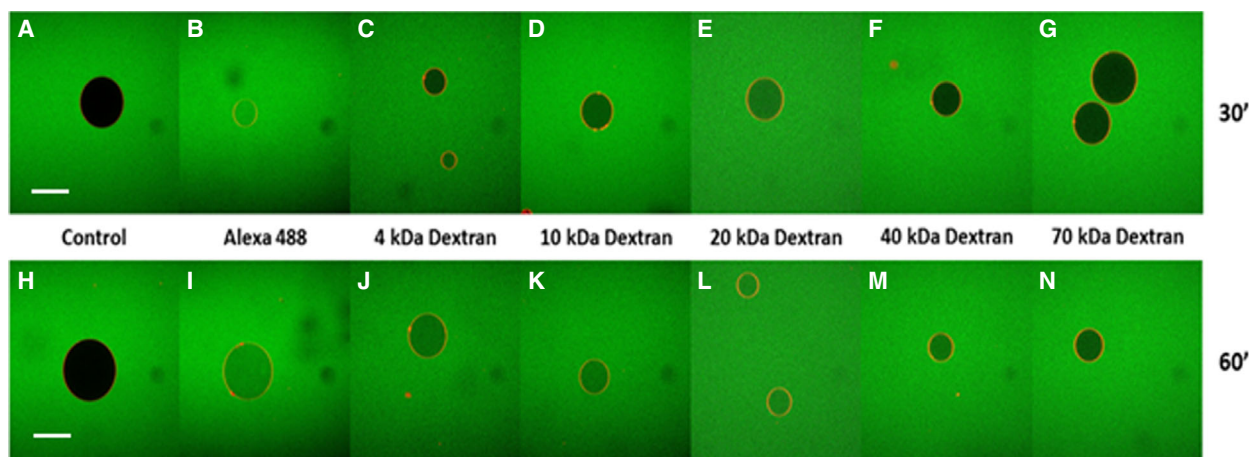
Fig. 7. Analysis by Confocal microscopy of the permeabilization to fluorescently-labeled solutes with diverse molecular sizes induced by ACT in DOPC:Chol 1 : 1 GUVs reveals that ACT forms pores with a larger effective size. Representative confocal microscopy images of GUVs in external solutions containing Alexa-Fluor-488, 4 kDa-FITC-Dextran, 10 kDa-FITC-Dextran, 20 kDa-FITC-Dextran, 40 kDa-FITC-Dextran, or 70 kDa-FITC-Dextran incubated in the absence (control), or presence of 200 nM ACT. Images were taken 30 min (subpanels a–g) or 60 min (subpanels h–n) after mixing the components. The filling of the lumen of GUVs with the corresponding fluorescent probe (green) corresponds to permeabilized vesicles. Controls correspond to untreated GUVs, and are seen of black color due to lack of fluorescence probe in the vesicle lumen, indicating that remain impermeable. Vesicle bilayer was labeled with PE-rhodamine (Sigma) at 1% (molar ratio), a fluorescently labeled phospholipid that was added at 0.5% (red color). For statistical analysis, we sampled 200 vesicles in each experiment and repeated each experiment three times. Scale bar (in white color) in subpanels a and h represents 20 μm.

To calculate the filling degree for each single vesicle, we measured the average fluorescence intensity of each fluorophore inside each individual GUV, and in the external medium, either for controls or for the cholesterol-containing GUVs treated with ACT (200 nM). We arbitrarily classified as nonpermeabilized the vesicles with permeabilization values lower than 10%. 200 vesicles were sampled in each experiment for the statistical analysis, and each experiment was repeated three times. The distribution of the degree of filling for each fluorophore is shown in Fig. 8, which evidences quantitatively the conclusions drawn from Fig. 7, this is, that after 1-h treatment at RT ACT forms, in significantly high number of DOPC:Chol (1 : 1 molar ratio) GUVs, pores that are permeable to very large molecular weight fluorescently labeled dextrans (40 kDa FITC-Dextran and 70 kDa FITC-Dextran). By contrast, we had previously found that the pores formed by ACT in pure DOPC GUVs under identical experimental conditions (200 nM ACT incubated for 60 min with DOPC GUVs) had an effective diameter of about 6.0 nm [18] since at this toxin dose only the FITC-Dextran 20 kDa could enter into the GUVs. Our present results with the cholesterol-containing vesicles indicated thus that the pores formed by ACT in the presence of the sterol evolve into very large holes. This was fully consistent with the observed enhancement by cholesterol in the rate and extent of permeabilization determined in LUVs (Fig. 1).

From the distribution of the filling degree at single-GUV level, one can have an idea on which of the two general permeabilization mechanisms, namely, 'all-or-none' or 'graded' [26], is followed by a given pore-forming agent. When the vesicles in the sample show only two states, either impermeable or totally permeabilized, then the mechanism is considered 'all-or-none'. Instead, when the individual GUVs show a varying filling degree the mechanism is considered 'graded'. 'All-or-none' permeabilization is characterized by strong cooperativity in permeabilization and usually involves formation of stable discrete-sized pores. In contrast, 'graded' permeabilization is not cooperative and exhibits slower kinetics, which leads to partial filling of the individual liposomes [26]. From data in Fig. 8, we could infer that ACT follows a graded mechanism of GUV permeabilization, and that the pores formed by the toxin are most likely proteolipidic [27].

Cholesterol favors ACT insertion into lipid monolayers

To explore whether cholesterol, besides enhancing ACT binding to lipid bilayers, might also affect toxin insertion into membranes which could be necessary for oligomerization, we used the monolayer technique. This methodology allows the direct observation of the insertion phenomenon, separated from further changes in
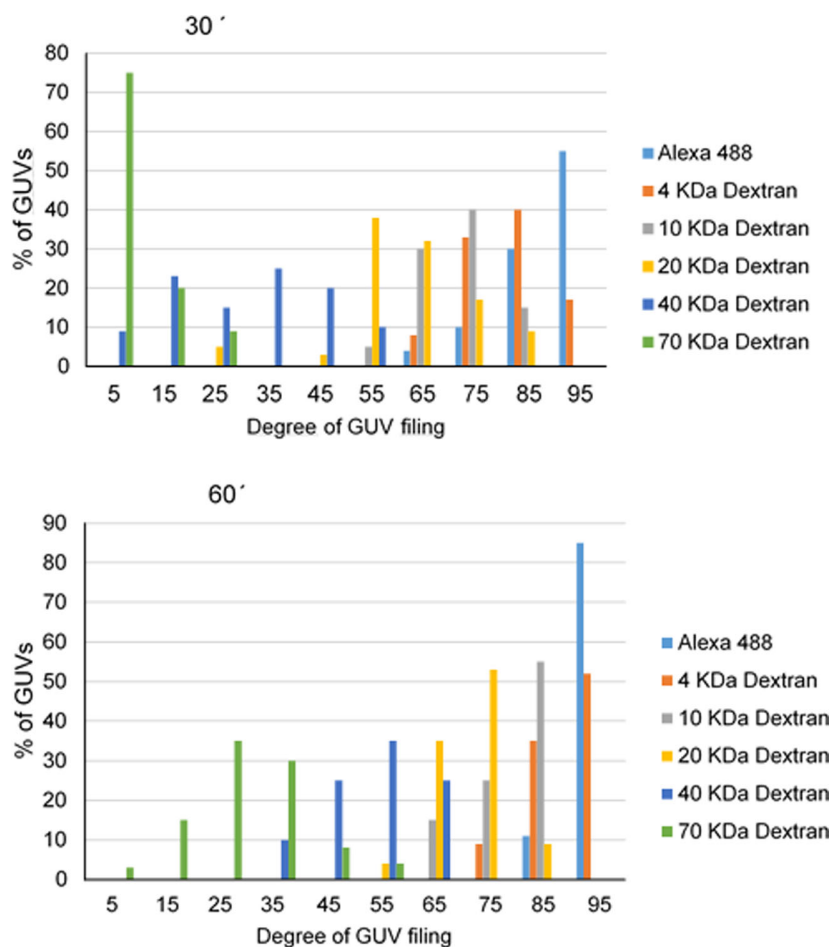
Fig. 8. Distribution of the degree of filling of individual DOPC:Chol 1 : 1 GUVs to fluorophores of different size. Alexa-Fluor-488, 4 kDa-FITC-Dextran, 10 kDa-FITC-Dextran, 20 kDa-FITC-Dextran, 40 kDa-FITC-Dextran, or 70 kDa-FITC-Dextran after treatment with ACT for 30 min (upper panel) or for 1 h (lower panel). In each of three independent experiments, 200 vesicles were analyzed per condition. The degree of filling was calculated for each individual vesicle from 200 GUVs measuring the fluorescence intensity of each fluorophore inside the vesicle and in the external medium. We arbitrarily classified as nonpermeabilized the GUVs with permeabilization values lower than 10%.

lipid architecture because, by design, the monolayer cannot undergo the 3D membrane restructuring that would be essential for altering the membrane-permeability barrier. Thus, the lipid monolayer studies enabled a scrutinizing of the insertion step itself apart from the membrane lysis that would subsequently occur.

Firstly, insertion of ACT at the water–air interface was measured, which yielded an increase of $\approx$ 20 mN·m^{-1} at ACT concentrations above 200 nm, indicating that ACT has amphipathic character (data not shown). The experiments shown in Fig. 9 were performed with monolayers of pure DOPC, or with two different cholesterol proportions, DOPC:Chol 2 : 1 and DOPC:Chol 1 : 1 molar ratio, being extended at the air/water interface of a Langmuir balance at an initial surface pressure (π_0) of 22 mN·m^{-1}. ACT (200 nm) was injected into the subphase. The results show that ACT can insert into the three different monolayers, which is manifested by an increase in the monolayer surface pressure (π) (Fig. 5, left panel). Interestingly, in the presence of cholesterol the increments of the surface pressure values were significantly higher and proportional to the sterol amount in

the monolayer ($\Delta\pi$ (π- π_i) were 5.7 mN·m^{-1} for DOPC, 6.6 mN·m^{-1} for DOPC:Chol 2 : 1, and 8.9 mN·m^{-1} for DOPC:Chol 1 : 1), indicating in principle that toxin insertion is favored in the membranes containing cholesterol. The presence of cholesterol in the lipid composition of the extended monolayer not only affected to the ACT-induced change of the monolayer lateral pressure, but also to the kinetics of ACT insertion, which became faster in the presence of cholesterol.

From the increase in surface pressure ($\Delta\pi$) upon ACT insertion, measured at various initial pressures (π_i), we constructed a critical pressure (exclusion pressure) plot (Fig. 9, right panel). Higher initial monolayer surface pressures correlate with higher lipid packing densities and hinder protein insertion. From the intersection of the plots with the abscissa axis, we can calculate the value of the critical pressure (π_c), that is, the initial surface pressure beyond which the protein can no longer insert into the monolayer. This parameter gives information about the avidity of each toxin for the monolayer [29]. The π_c values determined for ACT insertion were 27.33 mN·m^{-1} for pure DOPC
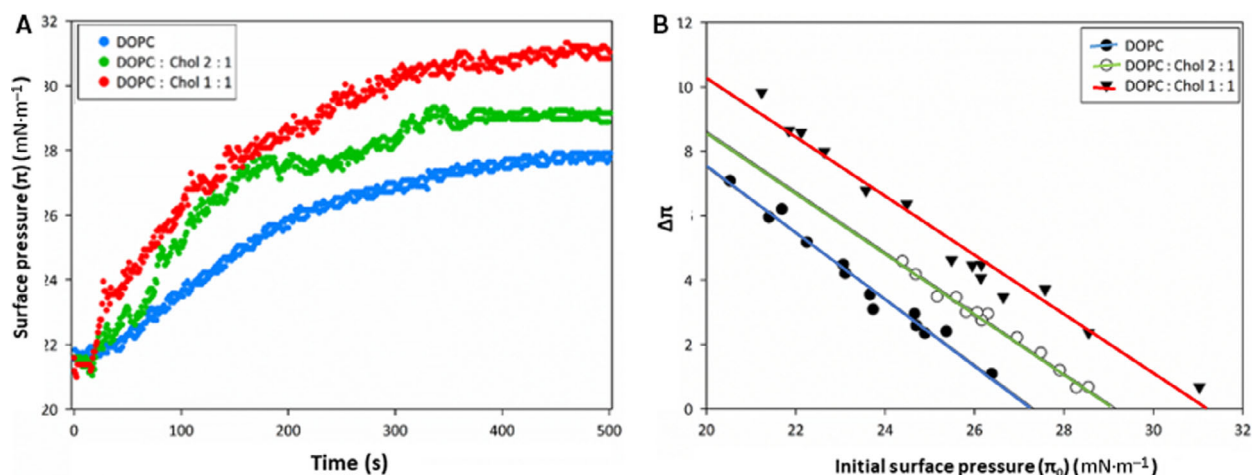
Fig. 9. Insertion of ACT into lipid monolayers of different lipid composition. (A) Changes in the surface pressure (π) after insertion of ACT (200 nM) into lipid monolayers of pure DOPC (in blue), or with two different cholesterol proportions, DOPC:Chol 2 : 1 (in green) and DOPC: Chol 1 : 1 (in red) molar ratio. Initial surface pressure (π_0) was set at 22 mN·m^{-1}. (B) Variations in the lateral pressure ($\Delta\pi = \pi - \pi_0$) at different initial surface pressure (π_0) in the range of 20–31 mN·m^{-1} recorded after addition of ACT (200 nM) to the monolayers prepared in buffer with CaCl$_2$. Data represent the mean values of at least three independent experiments.

monolayers, 29.17 mN·m^{-1} for the DOPC:CHOL 2 : 1 mixture, and 31.2 mN·m^{-1} for the DOPC:CHOL 1 : 1 mixture suggesting a favored ACT insertion into the cholesterol-containing monolayers.

Analysis by Atomic Force Microscopy of ACT inserted into cholesterol-containing supported lipid bilayers

To have more details on ACT insertion into cholesterol-containing membranes, we performed AFM analysis (room temperature) of supported lipid bilayers prepared from proteoliposomes containing ACT (2000 : 1 lipid: protein molar ratio). In these experiments, we used palmitoyloleylphosphatidylcholine (POPC):Chol (1 : 1 molar ratio) liposomes instead of DOPC: Chol (1 : 1 molar ratio) vesicles to prepare ACT-containing proteoliposomes. This was so to improve the stability of the liposomes and proteoliposomes extended onto the mica and because technical constraints of the AFM. Binding and permeabilization characteristics of ACT were very similar in both types of liposomes (not shown).

As shown in Fig. 10, the supported lipid bilayers containing ACT were very rich in structures protruding several nanometers, from ≈ 2.0 to ≈ 10.0, from the membrane plane (Fig. 10, upper panel). The detected ACT structures were heterogeneous in size and included lines, rings, and arc-shaped arrangements of protein, in addition to single dots (likely monomers), and some random aggregates. Previously, we found a similar pattern of heterogeneity in the assemblies formed by ACT

lytic pores in POPC supported bilayers [24]. Upon quantification of 1002 particles, the relative percentage determined for each structure was as follows: $63.5 \pm 9.9\%$ for monomers, $7.35 \pm 3.1\%$ for lines, $5.9 \pm 1.6\%$ for arcs, and $22.8 \pm 9.0\%$ for closed rings (Fig. 10, central panel). For comparison, in our previous study with POPC supported bilayers we had determined the following distribution for the different ACT assemblies: $72.5 \pm 6.3\%$ for monomers, $6.54 \pm 1.0\%$ for lines, $8.96 \pm 5.9\%$ for arcs, and $12.02 \pm 4.4\%$ for closed rings [18]. This indicated that in POPC:Chol (1 : 1 molar ratio) bilayers, at RT, the percentage of ACT oligomeric assemblies was about 30% greater, relative to the POPC bilayers, supporting the results obtained by BN-PAGE in which the relative abundancy of high molecular protein bands was greater for ACT toxin incubated with POPC:Chol (1 : 1) LUVs compared with the DOPC vesicles, and corroborating the idea that cholesterol promotes ACT oligomerization.

Other parameters determined from the AFM images were the height and diameter of the monomeric particle in each type of ACT assembly (monomer, line, arc, and ring) (Figs 11 and 12). These data revealed that as compared to the height of the monomers in the closed rings, which had a rather narrow and homogenous distribution predominating heights of around 2.8 nm, the single ACT monomers had a broad height distribution ranging between ≈ 2 nm and ≈ 10 nm over the membrane plane. Instead, the monomers heights in lines and arcs appeared to have an intermediate distribution
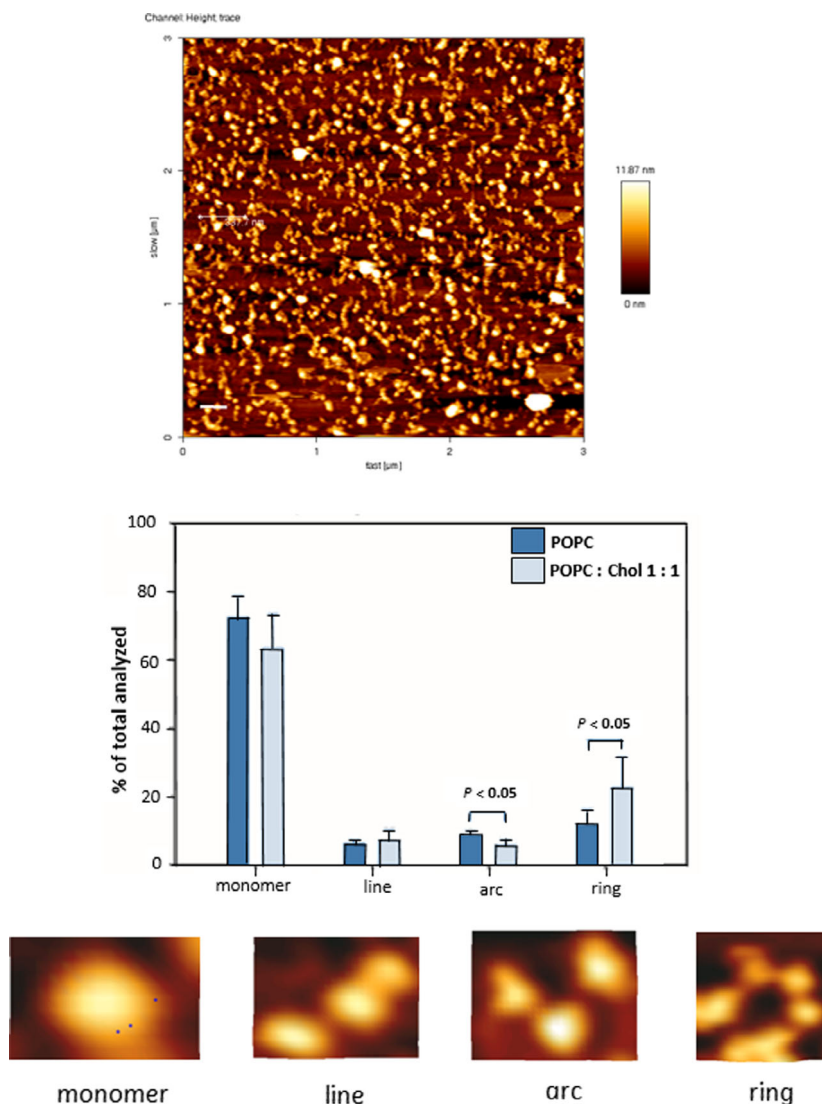
Fig. 10. Analysis by atomic force microscopy of the assemblies formed by ACT in supported lipid membranes composed of POPC and cholesterol. Representative AFM image (upper panel) of a supported lipid bilayer (SLB) prepared from ACT-containing proteoliposomes (POPC:Chol (1 : 1 molar ratio) liposomes reconstituted with ACT) (upper image). The SLB contains abundant and diverse ACT structures protruding several nanometers, from ≈ 2.0 to ≈ 10.0, from the membrane plane. Scale bar (in white color) at the bottom of the image corresponds to 200 nm. The detected ACT structures are heterogeneous in size, and included lines, rings, and arc-shaped arrangements of protein (lower panel). Quantitative analysis of the different structures (monomer, line, arc, and ring) determined for ACT on supported lipid bilayers SLBs of pure POPC or POPC: Chol (1 : 1 molar ratio) analyzed by AFM. Data show the percentage of each type of structure in all the measurements (central panel). The results are presented as mean $\pm$ S.D. Levels of significance of the differences between groups were determined by a two-tailed Student's *t*-test, and a confidence level of greater than 95% ($P < 0.05$) was used to establish statistical significance.

(3.0–6.0 nm). These differences in height likely reflect different degrees of penetration of the ACT structures into the lipid bilayer and suggest that to assemble into higher order structures (oligomers full rings) the ACT monomers might require a deeper insertion into the lipid bilayer.

The diameter of the monomeric particle in the different ACT assemblies showed a progressive decrease in size, from the ≈ 70 nm for the monomer alone, to ≈ 45 nm in the closed rings, passing through ≈ 50 nm in lines and arcs (Fig. 11). Recently, other group has determined by small angle x-ray scattering SAXS that the ACT monomer in solution has a diameter of ≈ 14–15 nm [30]. Assuming this size, our data suggest that that the toxin would transit from a more or less 'compact' state in solution, to a more 'open' or 'extended' conformation upon binding to the membrane.

Interestingly, full rings visualized in the AFM images showed very large sizes, with apparent diameters of 187 ± 38 nm in the more external side (upper vestibule) of the pore, and of 94 ± 25 nm in the upper internal part (Fig. 13). The depth of the lesions (closed rings) ranged from ≈ 2.4 to 4.4 nm (with respect to the flat surface of the lipid bilayer). Because the value determined by AFM for membrane thickness was of about 5.27 ± 0.3 nm, the results suggested that, though being lytic, ACT pores formed in POPC:Chol supported lipid bilayers did not apparently span the lipid bilayers, which may be explained by the lipid packing and ordering effect that moderate-high cholesterol concentrations induce in a disordered lipid bilayer such as POPC. This was interesting and supports again the idea that ACT pores are of toroidal characteristics and involve lipids [24].

Fig. 11. Determination of the height (in nm) of the monomeric particle in each of the different ACT assemblies (monomer, line, arc, or closed ring). Mean values are depicted as box-and-whisker plots (the ends of the whiskers represent standard deviations). A total of 1002 particles were measured for these determinations.
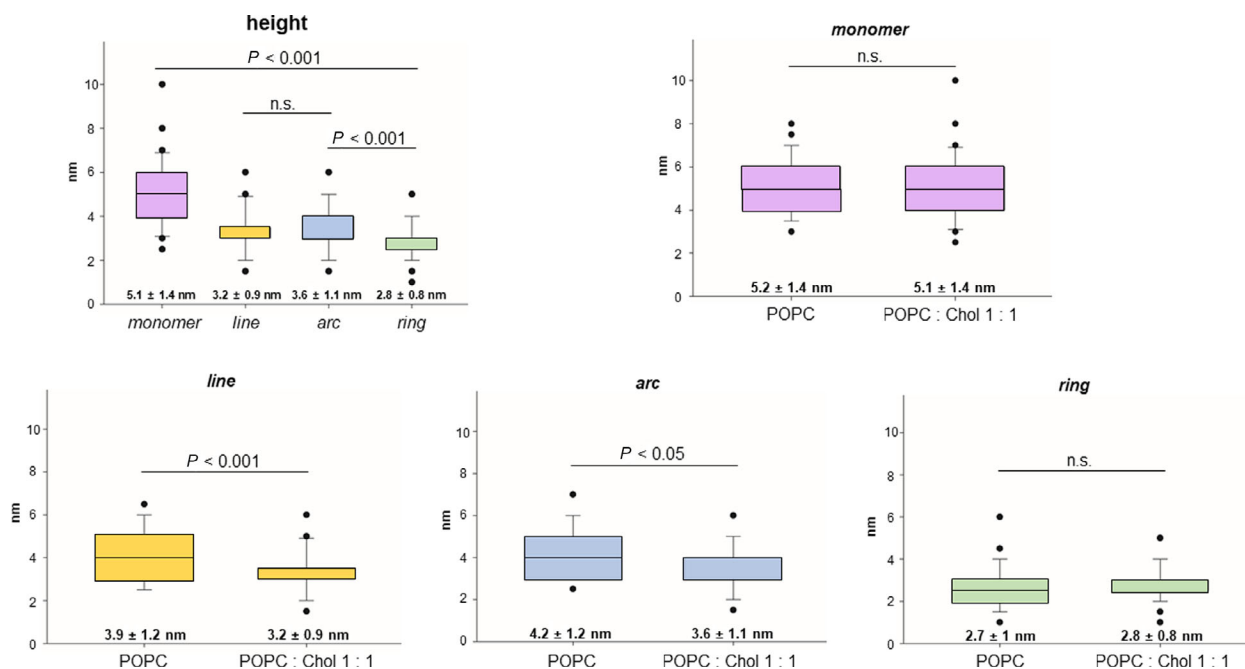

Fig. 12. Determination of the diameter (in nm) of the monomeric particle in each of the different ACT assemblies (monomer, line, arc, or closed ring). Mean values are depicted as box-and-whisker plots (the ends of the whiskers represent standard deviations). A total of 1002 particles were measured for these determinations.
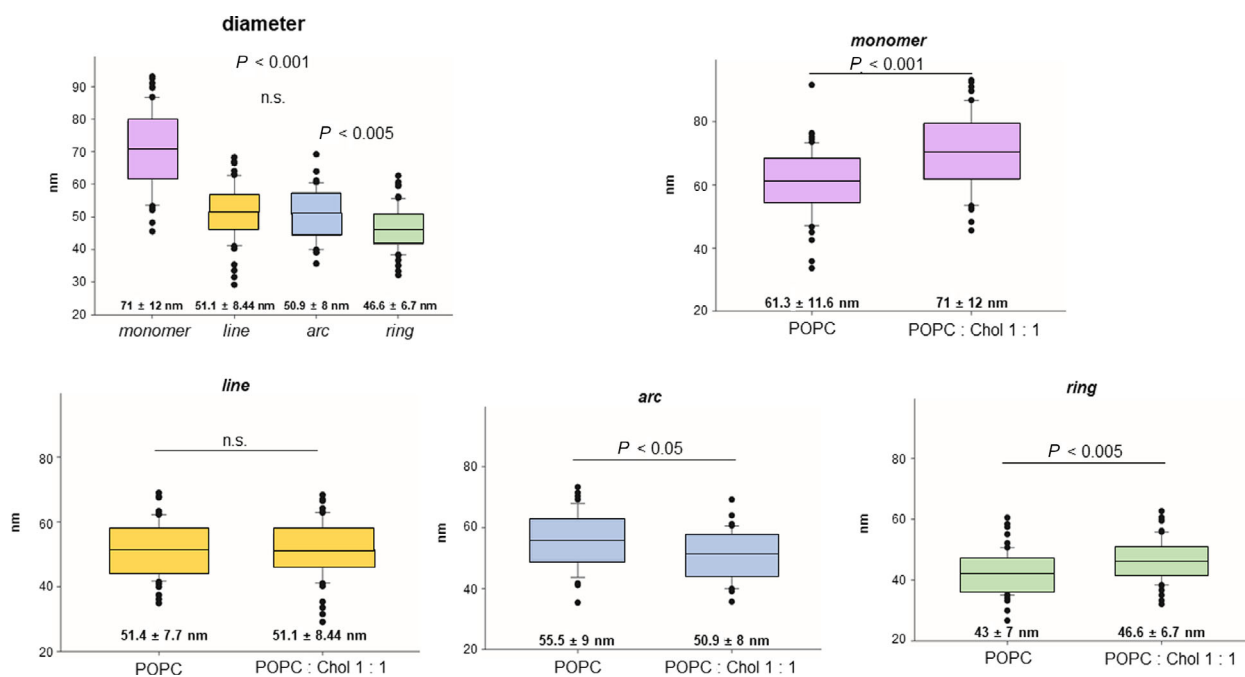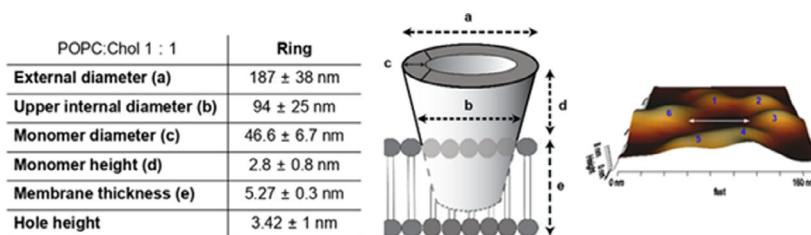
POPC:Chol 1 : 1	Ring
External diameter (a)	187 ± 38 nm
Upper internal diameter (b)	94 ± 25 nm
Monomer diameter (c)	46.6 ± 6.7 nm
Monomer height (d)	2.8 ± 0.8 nm
Membrane thickness (e)	5.27 ± 0.3 nm
Hole height	3.42 ± 1 nm

Fig. 13. Three-dimensional atomic force microscopy topography of ACT rings that pierce the POPC:Chol-supported lipid bilayer. Detailed 3D topographic analysis of ACT full rings, for which each constituent monomer has been numbered. Below, different parameters (external diameter, internal ring diameter, monomer diameter, monomer height, and ring 'hole' height) and their respective values are listed.
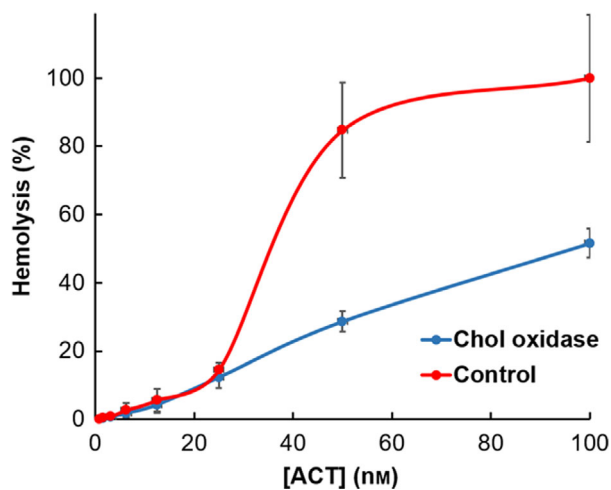

Fig. 14. Reduction of the cholesterol content in erythrocytes substantially decreases the ACT-induced hemolysis. Sheep erythrocytes (5×10^8 cells·mL^{-1}) were pretreated with cholesterol oxidase (1 U·mL^{-1}) for 30 min at 37 °C to decrease the cholesterol content available in the cell membrane. Then, ACT was added at different initial concentrations and incubations of 180 min were performed before determining the lysis percentage as described in the M&M section. Data depicted in the figure correspond to mean values ± SD. Three independent experiments were performed in duplicates ($n = 6$).

Decrease in the cholesterol-content notably reduces the ACT-induced hemolysis in erythrocytes

Erythrocytes have been broadly used as model cells to evaluate the lytic activity of ACT. Erythrocytes, which contain high amount of cholesterol (about $\approx 30\%$ of total lipids) [48,49], were used to evaluate the cholesterol relevance on the lytic activity of ACT on cells. Sheep erythrocytes (5×10^8 cells·mL^{-1}) were pretreated with cholesterol oxidase (1 U·mL^{-1}) for 1h at 37 °C. This is an enzyme that oxidizes the hydroxyl group at position 3 of the sterol, producing 4-cholestene-3-one.

This modification affects possible specific interactions of cholesterol with either lipids (particularly with sphingomyelin) or proteins, disrupting SM- and cholesterol-enriched lipid nanodomains. Cholesterol oxidase has been used as a suitable method to decrease the amount of cholesterol in a cell membrane.

As depicted in Fig. 14, pretreatment of the RBC with cholesterol oxidase provoked a substantial drop in the percentage of hemolysis, over a wide range of ACT concentrations, tripling the toxin dose required to induce the 50% hemolysis (D_{50}). These data suggested hence that cholesterol also plays an important role in the lytic activity of ACT on erythrocytes.

Discussion

Crucial role of cholesterol in facilitating structural rearrangements of proteins, upon association with the lipid bilayer, resulting in the spontaneous conversion of the protein from water-soluble to membrane-bound form, has been documented for several intrinsic proteins and bacterial protein toxins. The effect of cholesterol has been in most cases attributed to modification of the membrane properties by this sterol, involving lateral segregation of lipids and the consequent formation of nanodomains. Here, we show that cholesterol prominently enhances the lytic activity of adenylate cyclase toxin, ACT, by favoring insertion and consequently oligomerization of the toxin into the lipid bilayer, a step we previously found may be rate limiting in the mechanisms of membrane permeabilization by this toxin [24]. Moreover, we show that the enhanced toxin insertion is not primarily due to a lipid segregation effect of cholesterol, but rather to preferential interaction of the toxin with this sterol.

We have used several complementary biophysical techniques to scrutinize the different steps (binding, insertion, oligomerization) involved in the lytic activity of ACT, and this way have a more complete view on

the role of cholesterol in the different steps leading to pore formation by this RTX toxin. From the experiments of aqueous content leakage from LUVs, we can conclude that incorporation of cholesterol in pure DOPC liposomes makes those vesicles much more susceptible to permeabilization by ACT, proportionally to the amount of sterol included in the vesicles, and with a maximal effect induced by 50% cholesterol. We show that, cholesterol enhances both the extent and the rate of membrane permeabilization by ACT, since we determine that ACT not only requires about ten times less toxin concentration to permeabilize the DOPC:Chol (1 : 1 molar ratio) liposomes, relative to the DOPC LUVs ($D_{50} = 23$ nM vs 200 nM, respectively), but also that permeabilization of the cholesterol-containing vesicles is about 100 times faster. This suggests somehow that the fluid, liquid disordered (Ld), bulk lipid phase of the cell membrane (represented in our assays by pure DOPC lipid bilayers) would be poorly sensitive to ACT lytic action. Our data are consistent with previous early results obtained by other group in electrophysiology assays using black lipid membranes to detect pore formation by ACT, in which almost no conductance changes could be recorded when pure PC was used to form the lipid bilayers [23].

We determine that stimulation by cholesterol of membrane permeabilization by ACT is much more prominent at the lower toxin concentrations tested, while at higher toxin doses (˃ 100 nM) its enhancing effect disappears (Fig. 3), perhaps because the bilayer is saturated with toxin. Given that lysis by ACT pore-forming activity involves assembly of toxin monomers into the membrane [21,24,25], these data strongly suggest that ACT might require a critical monomer concentration at the membrane to oligomerize. Cholesterol might facilitate achievement of such minimal number of toxin molecules at lower initial ACT inputs by increasing ACT binding to the membrane, favoring this way toxin oligomerization and consequently vesicle permeabilization. We corroborate this hypothesis by directly visualizing that ACT protein bands of apparent high molecular masses (most likely corresponding to ACT oligomers) resolved in blue native gels (BN-PAGE) are more abundant in the cholesterol-containing vesicles than in the DOPC liposomes, and a direct binding assay that confirmed the greater toxin binding to the cholesterol-containing vesicles (Fig. 6). Additionally, we find that pre-incubation of ACT with different increasing concentrations of cholesterol-containing liposomes results in a greater inhibition of the lytic activity of ACT on red blood cells as compared to the more modest inhibition exerted by the DOPC vesicles. This indicates that a greater irreversible toxin interaction

(binding and/or insertion) to the DOPC:Chol liposomes leaves less free ACT monomers available to bind to erythrocytes, with the subsequent decrease in the toxin oligomerization and in the hemolysis of erythrocytes. Our results of lipid monolayers indicate that in the presence of cholesterol ACT inserts with a faster kinetics into the lipid monolayer. Besides, the toxin exerts a greater surface pressure increase ($\Delta\pi$) in the PC:Chol monolayers, for whatever initial lateral pressure imposed to the monolayer (πi). Also, a greater critical pressure (the initial surface pressure beyond which the protein can no longer insert into the monolayer) is obtained in the cholesterol-containing monolayers (Fig. 9), which all together suggests that ACT has more avidity for the cholesterol-containing monolayers and that a favored toxin insertion takes place in the presence of the sterol.

The results obtained with the cholesterol-containing GUVs have also been very revealing. They corroborate our previous finding that ACT follows a graded mechanism of permeabilization, also in presence of cholesterol, supporting our conclusion that ACT most likely forms dynamic proteolipidic pores (toroidal pores) in membranes [24]. We can thus say that cholesterol does not change the mechanisms of membrane permeabilization by ACT. We also find that ACT forms large pores permeable to dextrans of high molecular mass at shorter incubation times, which is consistent with the conclusion that cholesterol accelerates the toxin assembly to form oligomers and fully corroborates the results of permeabilization with LUVs. Also interestingly, we show that prolonging the incubation time the effective size of the solutes that can permeate to the GUVs is notably increased in the cholesterol-containing vesicles, with respect to the ACT pore size we determined previously into POPC GUVs [24], becoming into huge 'holes' of several nanometers wide, comparable to the large holes formed by the classical cholesterol-dependent cytolysins. This seems consistent with the dynamic nature of proteolipidic pores, which may form heterogeneous assemblies with an undetermined number of toxin monomers.

AFM data provide direct evidence of greater abundancy of ACT oligomers in the supported bilayers made of DOPC: Chol (1 : 1 molar ratio) as compared with the DOPC bilayers [24]. Interestingly, at difference with what we had observed previously for ACT monomers in lytic oligomers formed in pure DOPC bilayers, which were deeply inserted and spanned the lipid bilayer [24], in the DOPC: Chol lipid bilayer, ACT monomers in the oligomer are less deeply inserted, and do not completely traverse the lipid bilayer, but are fully lytic. This may be due to the

physical differences of the two lipid compositions. While pure DOPC is in a fluid liquid disorder state (Ld or Lα), a DOPC:Chol (1 : 1 molar ratio) lipid mixture adopts a single liquid ordered (Lo or Lβ) phase, with tightly packed lipids and greater thickness [43], mimicking, somehow, the more rigid Lo nanodomains enriched in SM and cholesterol ('rafts' that are believed to form in natural membranes [44-46]. Since the DOPC:Chol (1 : 1 molar ratio) lipid mixture forms a single lipid phase, this is, does not segregate into different lipid phases [47], we can rule out that the greater ACT insertion promoted by cholesterol is due to lipid phase segregation, but instead due to direct interaction of the sterol with ACT.

The cholesterol content of the plasma membrane of erythrocytes is ~ 45 mol% of total lipid [48]. When we decrease this cholesterol amount by treatment of the red blood cells with cholesterol oxidase, we show that the hemolysis induced by ACT notably decreases, and that higher toxins are required to lyse the cells. This is thus a strong indication that cholesterol is necessary both in model membranes as in cells to favor ACT insertion and oligomerization into the lipid bilayer, and ultimately to form lytic ACT pores.

Several proteins that interact with cholesterol, present in their sequences the so-called cholesterol recognition/interaction amino acid consensus (CRAC) motifs [49], which consist of the L/V-(X)(1–5)-Y-(X)(1–5)-R/K pattern, where (X)(1–5) represents between one and five residues of any amino acid, and the central Tyr is essential. Molecular modeling studies have shown that a CRAC motif belonging to transmembrane domains can have a good fit for cholesterol [50]. In other cholesterol-interacting proteins, a similar cholesterol-binding domain similar to CRAC, but with the opposite orientation along the polypeptide chain, has been identified: the CARC motif with K/R($X_{1–5}$)Y/F($X_{1–5}$)L/V R/K-(X)(1–5)-Y-(X)(1–5)-V/L pattern have been defined [66–68]. Existence of a specific interaction between cholesterol and several toxins from the RTX family has been recently noted, namely, in leukotoxin (LtxA) from *Aggregatibacter actinomytemcomitans* [31], in the *Escherichia coli* hemolysin (HlyA) [29], and in RtxA cytolysin from *Kingella kingae* [32]. All those pore-forming toxins have several conserved hydrophobic/amphipathic α-helixes, supposedly involved in pore formation, and in all of them cholesterol recognition amino acid sequences have been described. For the LtxA leukotoxin, two CRAC motifs were described, in or near the membrane-interacting region (residues 1–420), namely, CRAC (333–339) and CRAC (501–505) [31]. They showed that two peptides corresponding to

both CRAC motives bind Cho, but that only CRAC (333–339) competitively inhibits LtxA binding to this sterol and the ability of LtxA to kill Jurkat (Jn.9) cells. This motif is present in the hydrophobic domain (residues 1–420), which is strongly predicted to interact with membranes.

Up to now it had not been reported a specific interaction of the *Bordetella* ACT toxin with cholesterol. However, in view of the results of the present study that indicate a toxin-cholesterol interaction, it is strongly expected that ACT presents one or more 'functional' cholesterol recognition motifs, most likely situated in the hydrophobic/amphipathic membrane inserting helical region of the toxin (residues ≈ 500–700). From the analysis of ACT primary structure, numerous putative CRAC/CARC motifs can be predicted (Table 1). Interestingly, these putative cholesterol binding motives are disseminated, both at the N-terminal adenylate cyclase (AC) domain (residues ≈ 1 to 387), as at the C-terminal RTX hemolysin domain (390–1706). However, because the AC domain was reported not to interact with membranes [13], it seems reasonable to anticipate that the putative CRAC/CARC motives involved in cholesterol recognition are likely localize to the membrane inserting hemolysin region. Discerning which of them is/are relevant for cholesterol binding will be an interesting task for the near future.

Several authors in the field postulate that formation of ACT pores and translocation of the AC domain across cell membrane might be two independent and separable mutually exclusive membrane activities, accomplished by two different ACT conformers, one accounting for formation of membrane pores, and other, for AC domain translocation [21,51,52]. In view of our present results, it is very tempting to speculate that interaction of ACT with cholesterol (very likely through one or more of the predicted CRAC/CARC motives), facilitates the correct insertion into the membrane of certain ACT segments necessary for toxin oligomerization. Alternatively, ACT-cholesterol interaction might impede other interactions that might difficult protein assembly, but instead, facilitate AC domain translocation.

In conclusion, we provide here an ample set of evidences demonstrating that interaction of ACT with cholesterol enhances very notably its pore-forming activity by favoring toxin insertion and oligomerization, steps necessary for cell lysis. The presence in ACT sequence of several putative cholesterol recognition sequences lead us to hypothesize that ACT-cholesterol interactions involves very likely one or more of the predicted CRAC/CARC motives. Recognition of

Table 1. Identification of CRAC and CARC motifs in ACT sequence. The sequence of ACT (CyaA) was obtained in FASTA format from UniProt (http://www.uniprot.org/). A search for CRAC and CARC motifs was then performed with EMBROSS: fuzzpro (http://emboss.bioinformatics.nl/cgi-bin/emboss/fuzzpro). Sequences given as a search pattern were as follows: [LV]-X(1,5)-Y-X(1,5)-[RK], [RK]-X(1,5)-Y-X(1,5)-[LV].

Pattern		Amino acids	Sequence
[LV]-X(1,5)-Y-X(1,5)-[RK]	N-Terminal domain	161–166	VQYRRK
		215–224	VTDYLARTRR
		330–338	LKEYIGQQR
		343–348	VFYENR
	Hydrophobic region	626–638	LVQQSHYADQLDK
		653–661	LLAQLYRDK
	C-Terminal region	721–728	LANDYARK
		732–741	LGGPQAYFEK
		938–945	VSYAALGR
		1246–1255	LGVDYYDNVR
		1640–1652	LTVHDWYRDAHR
[RK]-X(1,5)-Y-X(1,5)-[LV]	N-Terminal domain	117–128	KERLDYLRQAGL
		348–352	RAYGV
		399–410	RQDSGYDSLDGV
	C-Terminal region	984–995	RTENVQYRHVEL

cholesterol in the membrane might facilitate insertion of certain ACT segments necessary for the toxin oligomerization, and/or perhaps, avoid other interactions that might difficult protein assembly, but instead facilitate AC domain translocation. Our study also provides a paradigm for the basis of cholesterol dependence for other pore-forming RTX toxins whose mechanism is enhanced by the presence of membrane cholesterol. Therefore, the enhancement in the conversion of pore-forming toxins to the membrane-inserted state may be a common effect of membrane cholesterol.

Materials and methods

Antibodies and reagents

Anti-adenylate cyclase toxin RTX domain mouse monoclonal antibody (MAb 9D4) was from Santa Cruz Biotechnology (Santa Cruz, CA, USA); anti-mouse FITC, Hoechst, and Mitotracker were from Invitrogen, Molecular Probes (Carlsbad, CA).

ACT purification

ACT was expressed in *Escherichia coli* XL-1 blue cells (Stratagene) transformed with pT7CACT1 plasmid, kindly provided by Dr. Peter Sebo (Institute of Microbiology of the ASCR, v.v.i., Prague, Czech Republic) and purified as described by Karst *et al.* [33].

Permeabilization determined as efflux of contents from large unilamellar vesicles

LUVs of different lipid composition were prepared by extrusion of multilamellar liposomes (MLV) following the method of Hope *et al.* [34]. Briefly, lipids in organic solution were mixed in the appropriate proportions, and the solvent was thoroughly evaporated. The resulting dry lipid film was hydrated in buffer, with gentle shaking, to form multilamellar vesicles. These were treated with 10 cycles of freezing and thawing, followed by 10 cycles of extrusion through polycarbonate filters (pore size, 0.1 μm; Nuclepore, Pleasanton, CA, USA).

Leakage of vesicular aqueous contents was assayed with ANTS and DPX entrapped in the liposomes according to Ellens *et al.* [41]. LUV were prepared in 70 mM NaCl, 12.5 mM ANTS, 45 mM DPX, and 20 mM Tris/HCl, pH 7.0. Nonentrapped probes were removed passing the LUV through a Sephadex G-75 column, eluted with 150 mM NaCl, 20 mM Tris/HCl, pH 7.0. After this preparation step, the final lipid concentration of the LUVs was determined using a method of determination of inorganic phosphorus [42]. Leakage assays were performed at 100 μm lipid in a total volume of 1 mL, with continuous stirring at 37 °C. Buffer was as above, with the addition of 10 mM CaCl2. The assay was started by adding the corresponding ACT dose. ANTS fluorescence was recorded continuously (λ_{ex} = 355 nm; λ_{em} = 520 nm). When leakage reached equilibrium, Triton X-100 was added (final concentration 0.1% w/v) to induce 100% release. Percent release was computed as follows:

$$\% \text{ release} = [(F_f - F_0)/(F_{100} - F_0)] \times 100,$$

where F_f, F_{100}, and F_0 were the respective fluorescence intensities observed after addition of ACT, after addition of Triton X-100, and before any addition.

Two other parameters were calculated from our experiments, namely, D_{50} and t_{50}. D_{50} that corresponds to the toxin concentration required to induce 50% permeabilization was calculated for each lipid composition from data depicted in Fig. 1. t_{50} (s) (Fig. 1C) indicates the time required for the toxin (at 100 nM concentration, an ACT dose broadly used to assay the hemolytic activity of this toxin) to induce 50% permeabilization of liposomes of a given lipid composition. It was calculated as the average of the values obtained from individual time course recordings such as the ones shown in Fig. S2.

Measurements of surface pressure with lipid monolayers

Surface pressure experiments were performed with a Micro-Trough-S system from Kibron (Helsinki, Finland) at 37 °C with constant stirring. The aqueous phase, or subphase, consisted of 150 mM NaCl, 20 mM Tris, 10 mM CaCl2, pH 8 buffer. The corresponding lipid or lipid mixture, dissolved

in chloroform/methanol (2 : 1, v/v), was gently spread over the surface of a Teflon microthrough containing 200 μL of subphase until the desired initial surface pressure was attained. The protein (250 nM) was injected with a micropipette into the subphase bulk. The increment in surface pressure against time was recorded until a stable signal was obtained. All the experiments were repeated at least three times for each lipid monolayer to ensure consistent results.

Measurement of Giant Unilamellar Vesicles (GUV) permeabilization as influx of fluorescent solutes

To prepare GUVs of different lipid composition, either dioleylphosphatidylcholine (DOPC) or DOPC:Chol (1 : 1 molar ratio), we followed the method developed by Angelova and Dimitrov [35]. Following the same protocol as in Montes and cols [37], we used a special temperature-controlled chamber previously described by Bagatolly and Gratton [36]. Before immersion in 200 μL sucrose (300 mM in H$_2$O), 6 μg of lipid mixture dissolved in chloroform was spread on platinum electrodes in the electroformation chamber and then allowed to dry. Electroformation proceeded for 2 h at 10 Hz, followed by 40 min at 2 Hz. To label the lipid bilayer of the GUVs, we used rhodamine-PE (0.25%). After vesicle formation, the chamber was left to settle at room temperature. To visualize the entry of the different fluorescent molecules to the lumen of the GUVs, the chamber was placed on an inverted confocal fluorescence microscope (Nikon Eclipse TELADO; Nikon, Japan). The excitation wavelengths were set at 488 nm (Alexa Fluor 488), 514 nm (Rhodamine-PE), and 490 nm (FITC-Dextrans). The fluorescence signal was collected into two different channels with band pass filters of 515/30 nm and 590/94 nm. The objective used was a 63X oleo immersion with a NA of 1.2. Image treatment was performed with the FIJI software.

The degree of GUV filling (*P*) was calculated as follows:

$$P = \frac{F_{int}}{F_{out}} \times 100.$$

where F_{int} and F_{out} are the average fluorescence intensities inside and outside a GUV at time *t*. We arbitrarily set to < 10% the threshold for classifying GUVs as nonpermeabilized. Several hundred GUVs were analyzed per experiment (≈ 200 per condition and experiment).

Blue-Native (BN-PAGE) Electrophoresis and western blotting

LUVs of different lipid composition, either DOPC or DOPC:Chol (1 : 1 molar ratio), were exposed to ACT (lipid:protein molar ratio of 2000 : 1) for 30' at 37°. After

this incubation period and to separate the ACT bound to the vesicles from the unbound toxin, the samples were submitted to ultracentrifugation in a sucrose gradient following the method described in [38] with minor modifications. Briefly, samples containing rhodamine-labeled liposomes (control untreated LUVs or toxin-treated LUVs) were adjusted to a sucrose concentration of 1.4 M in a final volume of 300 μL, and subsequently overlaid with 400- and 300-μL layers of 0.8 and 0.5 M sucrose, respectively. The gradient was centrifuged at 436 000 × *g* for 1 h in a TLA 120.2 rotor (Beckman Coulter, Brea CA, USA). After centrifugation, the toxin-containing fraction was collected.

Native gradient gels were manually prepared in a Mini-PROTEAN 3 Multi-Casting Chamber coupled to a Model 485 Gradient Former, both provided by Bio-Rad (CA, USA). The gels were prepared with an acrylamide gradient from 2 to 12% using two mixtures containing Gel buffer 3X (75 mM imidazole, 1.5 M 6-aminohexanoic acid, pH = 7), AB3-mix (48 g acrylamide and 5 g bisacrylamide in 100 mL water), and glycerol at a final concentration of 20% (v/v) only in the case of the mixture with a higher percentage of acrylamide. To both mixtures 10% APS and TEMED were added to proceed with polymerization.

Blue native polyacrylamide gel electrophoresis (BN-PAGE) was carried out essentially as described by Wittig *et al.* [39,40]. NativePAGE™ Sample Buffer (Thermo Fisher Scientific, MA, USA) was added to the samples, which were then loaded onto the gradient gels. A mixture of 50 mM Tricine and 7.5 mM imidazole at pH = 7 was used as cathode buffer, and 25 mM imidazole at pH = 7.0 as anode buffer. Gel running was performed at 4 °C for 1 h to 150 V, followed by 250 V for another additional hour at 4 °C. To estimate the molecular sizes of the bands, we used calibration curves prepared with native protein standards (NativeMark ™ Unstained Protein Standard, Thermo Fisher Scientific, MA, USA). After electrophoresis, the separated proteins were electroblotted onto Immobilon-P membranes (Merck Millipore), using native cathode buffer, and then detected by the indicated antibodies, and visualized by immunoperoxidase staining. The Quantity One® Image Analyzer software program (Bio-Rad) was used for quantitative densitometric analysis.

Flotation assay in sucrose gradient

ACT was incubated for 30 min with rhodamine-labeled DOPC or DOPC:Chol (1 : 1 molar ratio) liposomes (0.5% Rho-PE) at a lipid:protein ratio of 2000 : 1 in buffer containing 150 mM NaCl, 2 mM CaCl$_2$, and 20 mM Tris/HCl pH 8.0. After the incubation time, the unbound toxin was separated using a flotation assay in sucrose gradient. Briefly, samples containing rhodamine-labeled liposomes (control untreated LUVs or toxin-treated LUVs) were adjusted to a sucrose concentration of 1.4 M in a final

volume of 300 μL, and subsequently overlaid with 400- and 300-μL layers of 0.8 and 0.5 M sucrose, respectively. The gradient was centrifuged at 436 000 × *g* for 1 h and 4°C in a TLA 120.2 rotor (Beckman Coulter, Brea CA, USA). After centrifugation, the toxin-containing fraction was collected. Liposome-associated AC activity was then determined (binding) for each type of liposomes. AC activity assay was performed at 30°C in presence of 1 mM ATP and 0.1 μM calmodulin, 20 mM MgCl$_2$, 2 mM CaCl$_2$, and 30 mM Tris/HCl pH 7.4. cAMP was quantified using a cAMP ELISA kit (ENZO). Activities are expressed as percentages of intact free toxin activity and represent average values ± S.D. from three independent experiments.

Hemolysis assays

Hemolysis assays were performed on 96-well plates. Briefly, serial dilutions of ACT (starting at 100 nM) in assay buffer (20 mM Tris pH 8.0, 150 mM NaCl, 2.0 mM CaCl$_2$) were prepared, onto which an equal volume of erythrocytes at a density of 5×10^8 cells·mL^{-1} were added, and the mixtures incubated at 37°C for 180 min under constant stirring. At the end of the incubation time, the plates were centrifuged (2000 × *g*, 10 min, 4 °C) and the supernatant absorbance was measured at 412 nm. The blank (0% hemolysis) corresponded to erythrocytes incubated in buffer without toxin and 100%, and 100% hemolysis was obtained by adding Triton X-100 (0.1%) to the erythrocyte suspension.

Statistical analysis

All measurements were performed at least 3 times, and results are presented as mean ± S.D. Levels of significance of the differences between groups were determined by a two-tailed Student's *t*-test, and a confidence level of greater than 95% ($P < 0.05$) was used to establish statistical significance.

Acknowledgments

Conflict of interest

The authors declare that they have no conflicts of interest with the contents of this article. The funding sources had no involvement in the study design nor in the collection, analysis, and interpretation of data nor in the writing of the report or in the decision to submit the article for publication.

Data accessibility

All the data are contained within the article and in the Supporting Information.

Author contribution

DGB, KBU, JA, CM, and HO planned the experiments; DGB, KBU, JA, and CM performed experiments and analyzed the data; HO wrote the paper.

Peer Review

The peer review history for this article is available at https://publons.com/publon/10.1111/febs.16107.

References

1 Liscum L & Underwood K (1995) Intracellular cholesterol transport and compartmentation. *J Biol Chem* **270**, 15443–15446. https://doi.org/10.1074/jbc.270.26.15443.

2 Simons K & Ikonen E (2000) How cells handle cholesterol. *Science* **290**, 1721–1726. https://doi.org/10.1126/science.290.5497.1721.

3 Mouritsen O & Zuckermann M (2004) What's so special about cholesterol? *Lipids* **39**, 1101–1113. https://doi.org/10.1007/s11745-004-1336-x.

4 Gilbert R (2010) Cholesterol-dependent cytolysins. *Adv Exp Med Biol* **677**, 56–66.

5 Epand R (2006) Cholesterol and the interaction of proteins with membrane domains. *Prog Lipid Res* **45**, 279–294. https://doi.org/10.1016/j.plipres.2006.02.001.

6 Martín C, Requero M, Masin J, Konopasek I, Goñi FM, Sebo P & Ostolaza H (2004) Membrane restructuring by Bordetella pertussis adenylate cyclase toxin, a member of the RTX toxin family. *J Bacteriol* **186**, 3760–3765.

7 Carbonetti NH (2010) Pertussis toxin and adenylate cyclase toxin: key virulence factors of Bordetella pertussis and cell biology tools. *Future Microbiol* **5**, 455–469.

8 Carbonetti NH & Artamonova GV (2005) Pertussis toxin and adenylate cyclase toxin provide a one-two punch for establishment of bordetella pertussis infection of the respiratory tract. *Infect Immun* **73**, 2698–2703.

9 Guermonprez P, Khelef N, Blouin E, Rieu P, Ricciardi-Castagnoli P, Guiso N, Ladant D & Leclerc C (2001) The adenylate cyclase toxin of Bordetella pertussis binds

to target cells via the alpha(M)beta(2) integrin (CD11b/CD18). *J Exp Med* **193**, 1035–1044.

10 Confer DL & Eaton JW (1982) Phagocyte impotence caused by an invasive bacterial adenylate cyclase. *Science* **217**, 948–950.

11 Welch RA (1991) Pore-forming cytolysins of gram-negative bacteria. *Mol Microbiol* **5**, 521–528.

12 Linhartová I, Bumba L, Mašn J, Basler M, Osicka R, Kamanová J, Procházková K, Adkins I, HejnováHolubová J, Sadílková L *et al.* (2010) RTX proteins: A highly diverse family secreted bya common mechanism. *FEMS Microbiol Rev* **34**, 1076–1112.

13 Glaser P, Sakamoto H, Bellalou J, Ullmann A & Danchin A (1988) Secretion of cyclolysin, the calmodulin-sensitive adenylate cyclase-haemolysin bifunctional protein of Bordetella pertussis. *EMBO J* **7**, 3997–4004.

14 Karst JC, Barker R, Devi U, Swann MJ, Davi M, Roser SJ, Ladant D & Chenal A (2012) Identification of a region that assists membrane insertion and translocation of the catalytic domain of Bordetella pertussis CyaA toxin. *J Biol Chem* **287**, 9200–9212.

15 Ladant D & Ullmann A (1999) Bordetella pertussis adenylate cyclase: A toxin with multiple talents. *Trends Microbiol* **7**, 172–176.

16 Hackett M, Guo L, Shabanowitz J, Hunt DF & Hewlett EL (1994) Internal lysine palmitoylation in adenylate cyclase toxin from Bordetella pertussis. *Science* **266**, 433–435.

17 Baumann U, Wu S, Flaherty KM & McKay DB (1993) Three-dimensional structure of the alkaline protease of Pseudomonas aeruginosa: A two-domain protein with a calcium binding parallel beta roll motif. *EMBO J* **12**, 3357–3364.

18 Chenal A, Iñaki Guijarro J, Raynal B, Delepierre M & Ladant D (2009) RTX calcium binding motifs are intrinsically disordered in the absence of calcium implication for protein secretion. *J Biol Chem* **284**, 1781–1789.

19 Holland IB, Schmitt L & Young J (2005) Type 1 protein secretion in bacteria, the ABC-transporter dependent pathway. *Mol Membr Biol* **22**, 29–39.

20 Hewlett EL, Donato GM & Gray MC (2006) Macrophage cytotoxicity produced by adenylate cyclase toxin from Bordetella pertussis: more than just making cyclic AMP! *Mol Microbiol* **59**, 447–459.

21 Basler M, Knapp O, Masin J, Fiser R, Maier E, Benz R, Sebo P & Osicka R (2007) Segments crucial for membrane translocation and pore-forming activity of Bordetella adenylate cyclase toxin. *J Biol Chem* **282**, 12419–12429.

22 Gray M, Szabo G, Otero AS, Gray L & Hewlett E (1998) Distinct mechanisms for K+ efflux, intoxication, and hemolysis by Bordetella pertussis AC toxin. *J Biol Chem* **273**, 18260–18267.

23 Benz R, Maier E, Ladant D, Ullmann A & Sebo P (1994) Adenylate cyclase toxin (CyaA) of Bordetella pertussis. Evidence for the formation of small ion-permeable channels and comparison with HlyA of Escherichia coli. *J Biol Chem* **269**, 27231–27239.

24 González-Bullón D, Uribe KB, Largo E, Guembelzu G, García-Arribas AB, Martín C & Ostolaza H (2019) Membrane permeabilization by bordetella adenylate cyclase toxin involves pores of tunable size. *Biomolecules* **9**, 183.

25 Vojtova-Vodolanova J, Basler M, Osicka R, Knapp O, Maier E, Cerny J, Benada O, Benz R & Sebo P (2009) Oligomerization is involved in pore formation by Bordetella adenylate cyclase toxin. *FASEB J* **23**, 2831–2843.

26 Apellániz B, Nieva JL, Schwille P & García-Sáez AJ (2010) All-or-none versus graded: Single-vesicle analysis reveals lipid composition effects on membrane permeabilization. *Biophys J* **99**, 3619–3628.

27 Bleicken S, Landeta O, Landajuela A, Basañez G & García-Sáez AJ (2013) Proapoptotic Bax and Bak proteins form stable protein-permeable pores of tunable size. *J Biol Chem* **288**, 33241–33252.

28 Tweten RK (2001) Clostridium perfringens beta toxin and Clostridium septicum alpha toxin: their mechanisms and possible role in pathogenesis. *Vet Microbiol* **82**, 1–9.

29 Vazquez RF, Maté SM, Bakás LS, Fernández MM, Malchiodi EL & Herlax VS (2014) Novel evidence for the specific interaction between cholesterol and a-haemolysin of Escherichia coli. *Biochem J* **458**, 481–489.

30 Cannella SE, Ntsogo Enguéné VY, Davi M, Malosse C, Sotomayor Pérez AC, Chamot-Rooke J, Vachette P, Durand D, Ladant D & Chenal A (2017) Stability, structural and functional properties of a monomeric, calcium–loaded adenylate cyclase toxin, CyaA, from Bordetella pertussis. *Sci Rep* **7**, 42065.

31 Bumba L, Masin J, Fiser R & Sebo P (2010) Bordetella adenylate cyclase toxin mobilizes its beta2 integrin receptor into lipid rafts to accomplish translocation across target cell membrane in two steps. *PLoS Pathog* **6**, e1000901.

32 Brown AC, Balashova NV, Epand RM, Epand RF, Bragin A, Kachlany SC, Walters MJ, Du Y, Boesze-Battaglia K & Lally ET (2013) Aggregatibacter actinomycetemcomitans leukotoxin utilizes a cholesterol recognition/amino acid consensus site for membrane association. *J Biol Chem* **288**, 23607–23621.

33 Osickova A, Balashova N, Masin J, Sulc M, Roderova J, Wald T, Brown AC, Koufos E, Chang EH, Giannakakis A *et al.* (2018) Cytotoxic activity of Kingella kingae RtxA toxin depends on post-translational acylation of lysine residues and cholesterol binding. *Emerg Microbes Infect* **7**, 178.

34 Karst JC, Ntsogo Enguene VY, Cannella SE, Subrini O, Hessel A, Debard S, Ladant D & Chenal A (2014) Calcium, acylation, and molecular confinement favor

folding of Bordetella pertussis adenylate cyclase CyaA toxin into a monomeric and cytotoxic form. *J Biol Chem* **289**, 30702–30716.

35 Hope MJ, Bally MB, Webb G & Cullis PR (1985) Production of large unilamellar vesicles by a rapid extrusion procedure. Characterization of size distribution, trapped volume and ability to maintain a membrane potential. *Biochim Biophys Acta Biomembr* **812**, 55–65.

36 Angelova MI & Dimitrov DS (1986) Liposome electroformation. Faraday Discuss. *Chem Soc* **81**, 303–311.

37 Bagatolli LA & Gratton E (1999) Two-photon fluorescence microscopy observation of shape changes at the phase transition in phospholipid giant unilamellar vesicles. *Biophys J* **77**, 2090–2101.

38 Montes L, Alonso A, Goñi FM & Bagatolli LA (2007) Giant unilamellar vesicles electroformed from native membranes and organic lipid mixtures under physiological conditions. *Biophys J* **93**, 3548–3554.

39 Spearman P, Horton R, Ratner L & Kuli-Zade I (1997) Membrane binding of human immunodeficiency virus type 1 matrix protein *in vivo* supports a conformational myristyl switch mechanism. *J Virol* **71**, 6582–6592.

40 Wittig I, Braun H & Schägger H (2006) Blue native PAGE. *Nat Protoc* **1**, 418–428.

41 Ellens H, Bentz J & Szoka FC (1984) pH-induced destabilization of phosphatidylethanolamine-containing liposomes: role of bilayer contact. *Biochemistry* **23**, 1532–1538.

42 Fiske CH & Subbarow Y (1925) The colorimetric determination of phosphorus. *J Biol Chem* **66**, 375–379.

43 Ipsen JH, Karlstrom G, Mouritsen OG, Wennerstrom H & Zuckermann MJ (1987) Phase equilibria in the phosphatidylcholine-cholesterol system. *Biochim Biophys Acta* **905**, 162–172.

44 Simons K & Ikonen E (1997) Functional rafts in cell membranes. *Nature* **387**, 569–572.

45 Lingwood D, Kaiser HJ, Levental I & Simons K (2009) Lipid rafts as functional heterogeneity in cell membranes. *Biochem Soc Trans* **37**, 955–960.

46 Brown DA & London E (1988) Structure and origin of ordered lipid domains in biological membranes. *J Membr Biol* **164**, 103–114.

47 Flanagan JJ, Tweten RK, Johnson AE & Heuck AP (2009) Cholesterol exposure at the membrane surface is necessary and sufficient to trigger perfringolysin O binding. *Biochemistry* **48**, 3977–3987.

48 Owen JS, Bruckdorfer K, Day RC & McIntyre N (1982) Decreased erythrocyte membrane fluidity and altered lipid composition in human liver disease. *J Lipid Res* **23**, 124–132.

49 Li H & Papadopoulos V (1998) Peripheral-type benzodiazepine receptor function in cholesterol transport. Identification of a putative cholesterol recognition/interaction amino acid sequence and consensus pattern. *Endocrinology* **139**, 4991–4997.

50 Epand RM, Thomas A, Brasseur R & Epand RF (2010) Cholesterol interaction with proteins that partition into membrane domains: An overview. *Sub-Cell Biochem* **51**, 253–278.

51 Gray WC, Lee SJ, Gray LS, Zaretzky FR, Otero AS, Szabo G & Hewlett E (2001) Translocation specific conformation of adenylate cyclase toxin from Bordetella pertussis inhibits toxin-mediated hemolysis. *J Bacteriol* **183**, 5904–5910.

52 Osicková A, Osicka R, Maier E, Benz R & Šebo P (1999) An amphipathic a-helix including glutamates 509 and 516 is crucial for membrane translocation of adenylate cyclase toxin and modulates formation and cation selectivity of its membrane channels. *J Biol Chem* **274**, 37644–37650.